Fiber Optically Sensorized Multi-Fingered Robotic Hand

Leo Jiang[1], Kevin Low[1], Joey Costa[2], Richard J. Black[2], and Yong-Lae Park[3]

Abstract— We present the design, fabrication, and characterization of a fiber optically sensorized robotic hand for multi purpose manipulation tasks. The robotic hand has three fingers that enable both pinch and power grips. The main bone structure was made of a rigid plastic material and covered by soft skin. Both bone and skin contain embedded fiber optics for force and tactile sensing, respectively. Eight fiber optic strain sensors were used for rigid bone force sensing, and six fiber optic strain sensors were used for soft skin tactile sensing. For characterization, different loads were applied in two orthogonal axes at the fingertip and the sensor signals were measured from the bone structure. The skin was also characterized by applying a light load on different places for contact localization. The actuation of the hand was achieved by a tendon-driven under-actuated system. Gripping motions are implemented using an active tendon located on the volar side of each finger and connected to a motor. Opening motions of the hand were enabled by passive elastic tendons located on the dorsal side of each finger.

I. INTRODUCTION

The emergence of soft robotics is a key trend in the robotics field. Although conventional rigid body robotics has served well in automation and in controlled environments, as robotics expands to broader applications and mainstream consumers, the need for dexterous and adaptable systems that can accurately and safely interact with their surroundings is paramount to the advancement of robotics [1], [2].

The conventional approaches to robotics have resulted in robots that are capable of impressive tasks. The Robonaut, a humanoid robot made by NASA Johnson Space Center (JSC) exemplifies the sophistication of current robotics, with state-of-the-art tactile sensing, force sensing, and two seven-degrees-of-freedom (DOF) dexterous arms [3], [4]. However, even the state-of-the-art Robonaut presents important challenges for better integration of tactile perception, force control, and multi-fingered hand technologies. Particularly problematic is the lack of sensing capabilities, compared to natural organisms. For example, compared to insects, such as spiders, which have hundreds of mechanoreceptors in their

[1]Leo Jiang and Kevin Low are with the Department of Mechanical Engineering, Carnegie Mellon University, Pittsburgh, PA 15213, USA (E-mail: longlonj@andrew.cmu.edu, kylow@andrew.cmu.edu).

[2]Richard J. Black and Joey Costa are with Intelligent Fiber Optic Systems (IFOS) Corp., Santa Clara, CA, PA 15213, USA (E-mail: rjb@ifos.com, jc@ifos.com).

Yong-Lae Park is with the Robotics Institute in the School of Computer Science and the Department of Mechanical Engineering, Carnegie Mellon University, Pittsburgh, PA 15213, USA (E-mail: ylpark@cs.cmu.edu).
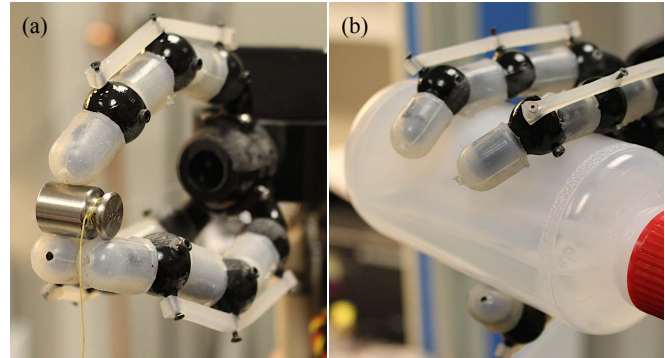
Fig. 1. Prototype of multi-fingered robotic gripper. (a) Pinch grip. (b) Power grip.

legs [5], [6], even the Robonaut has only 42 sensors in its hand and wrist module [4], [7]. This phenomenon extends to most contemporary robots, and, as a result of this drastic difference in sensor numbers, robots often appear relatively less capable of detecting and reacting to arbitrarily forces relative to its natural organism counterparts.

The approach we propose in this paper aims to bridge this gap by utilizing a combination of rigid structures and soft materials. Fig. 1 shows our prototype of a multi-fingered robotic hand with a combination of soft and rigid structures. Moreover, we introduce fiber optic strain sensors that have potential to improve force and touch sensing capabilities of robots [8], [9], [10], [11] by offering solutions to conventional force sensing methods, such as strain gages, force sensitive resistors, and pressure sensitive conductive polymer composites [12], [13], [14], [15], [16], [17]. Some of the major shortcomings of these methods are complicated wiring and a time-consuming manual installation process. Also, the wires are often fragile and susceptible to electromagnetic interference. These limitations contribute to the limited number of sensors in conventional robots.

For sensing, we used fiber Bragg grating (FBG) sensors that could detect minuscule strain changes by measuring shifts in reflection wavelength of an input light through the fiber optics [18], [19], [20]. The advantages of FBGs are structural robustness, immunity to electromagnetic interference, and high strain sensitivity. The proposed system uses two different sensing modalities: contact force sensing and tactile sensing. Force sensing is achieved through FBG sensors directly embedded in a rigid bone structure. The FBG sensors detect strain changes of the sensor-embedded structure caused by external forces applied. Tactile sensing, localization of contact points, is achieved through an FBG

array embedded in soft skin that covers the bone structure.

The actuation for each finger is achieved by an under-actuated system [21], [22], where each finger has two different types of tendon: active and passive. The active tendon, passing through the length of the finger, is used for active finger flexion. Tendon-driven under-actuated systems have demonstrated their actuation efficiency and mechanical simplicity in various robotic grippers and end-effectors [23], [24], [25], [26]. When the tension of the active tendon is released, the finger retracts due to the elastic passive tendon. The resulting under-actuation mechanism retains simplicity while having dexterous and lightweight characteristics.

II. DESIGN

The design philosophy for our fingers was simplicity in actuation, while not compromising richness and accuracy in sensing. This led us to employ an under actuated system with both force and touch sensing capabilities based on structural deformation.

A. Finger Design

The finger assembly was composed of three sections, a fingertip, a middle node, and a finger-base node, with cylindrical shapes, mimicking the skeletal structure of the human finger. The reason for emulating the human finger is that most objects and tools are designed and manufactured with the intent of being handled by human hands. By modeling after the human finger, we can eliminate the need to account for the majority of gripping scenarios. Fig. 2 shows the overall design of the finger and a photo of an actual prototype.

In comparison with human fingers, our robot fingers involve hollow shell structures of rigid bones, similar to the exoskeletons of arthropods [27], [28]. This type of shell structures not only provides a relatively high structural strength while significantly reducing weight and material, but also contributes to amplifying the structural deformation resulting in increase in sensitivity of the embedded strain sensors [9]. Another advantage of a hollow structure is that the rigid shell can protect fibers and cables for sensing and actuation that are internally routed through the structure.

B. Sensing Mechanism

We used FBG sensors in our prototype. Given broadband light excitation, each FBG reflects a narrow wavelength band centered on a wavelength λ that is characteristic of the FBG. The reflection wavelength λ shifts proportionally to strain experienced by the sensor, with sensitivity to axial strain up to approximately 1.2 pm at 1550 nm wavelength [29], [30], and the typical resolution of strain detection on the order of 0.1 $\mu\varepsilon$ or better [31]. This sensitivity allows FBG sensors to be used in areas that experience only modest stress and strains. Also, due to the flexibility of optical fibers, we can embed sensors in areas where conventional strain gauges would not have been feasible, such as at the fingertips.

In our system, two sensing modalities, force and touch, are detected by multiple FBGs embedded in different locations of each finger. Figs. 2-a and 2-b show the locations and
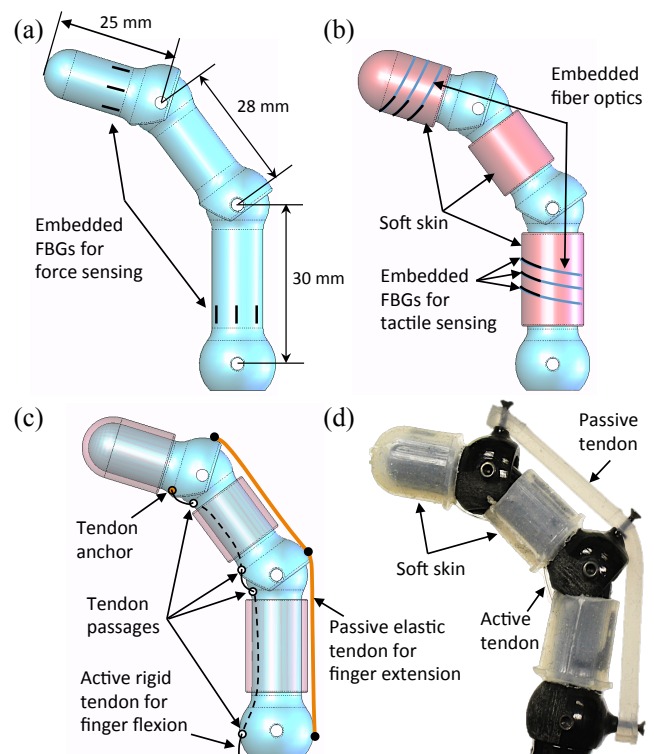

Fig. 2. Details of finger design for sensing and actuation. (a) Contact force sensing mechanism. (b) Touch sensing mechanism. (c) Actuation mechanism. (d) Actual prototype.

numbers of the FBGs embedded for force and tactile sensing, respectively. For force sensing, four FBGs at 90° intervals were embedded at the bases of the fingertip and the finger-base bones, for a total of eight FBGs in the bones. Details on the sensor configuration in the bone structure are shown in Fig. 3. For tactile sensing, an array of three FBGs was embedded in a helical way in the fingertip and the finger-base skins, for a total of six FBGs in the skins. Therefore, a total of16 FBGs were used in one finger. Although the bone FBGs provide force readings of the contacts based on the wavelength shifts, the skin FBGs provide only binary touch information since they are directly deformed by contacts, and the wavelength shift values may not be necessarily proportional to the magnitudes of the contact forces.

C. Actuation Mechanism

Each finger had two different tendons: an active tendon and a passive tendon. The active tendon was located at the volar side of the finger providing active grip (i.e.,, finger flexion) motions and forces when it was pulled. It was anchored at the base of the fingertip and routed down to the base of the finger through multiple filleted passages (holes). The active tendons were made of a flexible but inextensible nylon string (Trilene, Berkley) to ensure accurate force transmission. The passive tendon was located at the dorsal side of the finger and anchored at the base of each joint providing passive release (i.e., finger extension) motions and forces when the active tendon was released. The passive tendons were cast from
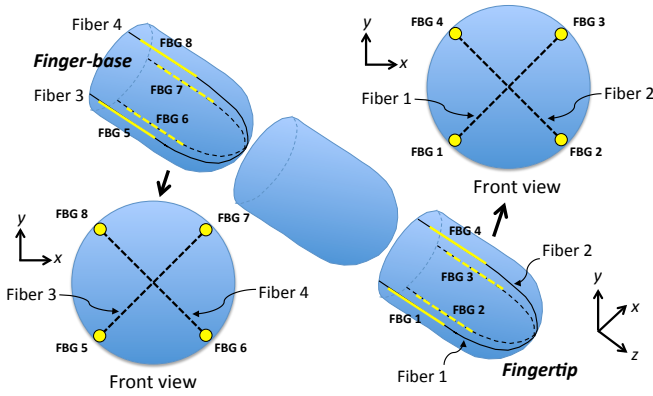
Fig. 3. FBG sensor configuration. Two optical fibers were embedded in the fingertip and the other two in the finger-base. Each fiber contained two FBGs for a total of eight FBGs in each finger.

Fig. 4. Three fingered robotic hand prototype. (a) Open and close motions. (b) Finger configuration.

a soft elastomer (EcoFlex-0030, Smooth-On) that ensures the repeatability of contraction over multiple stretches. The passive tendons help simplifying both design and control of the gripper. The under-actuated finger structure using two different tendons is shown in Fig. 2-c.

D. Gripper Design

Although the original plan was making an anthropomorphic five-fingered robotic hand, we decided to simplify the design to a three fingered gripper as an early prototype, as shown in Fig. 4-a. The design was influenced by the finger placement on the hand. As shown in Fig. 4-b, the positions of the fingers on the hand can be modified, so that we can find the optimal position for pinching and gripping. In doing so, we chose to place the fingers in a $150°$–$60°$–$150°$ configuration, since it gave the fingers adequate room to grip objects yet also allowed the fingers to pinch as it did not experience a large imbalance in force (F) while pinching. These features gave the hand a simple yet effective design. The tendons from all three fingers were fixed to the rotor of a relatively powerful servo motor (HS-5485HB, HiTEC) that provided simultaneous closing and opening motions of the three fingers.

III. FABRICATION

A. Bone Structure

The exoskeletal bone structure was 3-D printed (Connex30, Stratasys) using a rigid ultraviolet cured polymer material (VeroBlack, Stratasys) and held together through a combination of the two tendons and joint screws between the nodes. By using a 3-D printing technology, the complicated manufacturing process associated with multiple molding and casting steps shown in previous work [9] can be significantly simplified.

B. Soft Skin

The skin of the finger was cast using a highly deformable silicone elastomer (EcoFlex-0030, Smooth-On). The silicone at a liquid 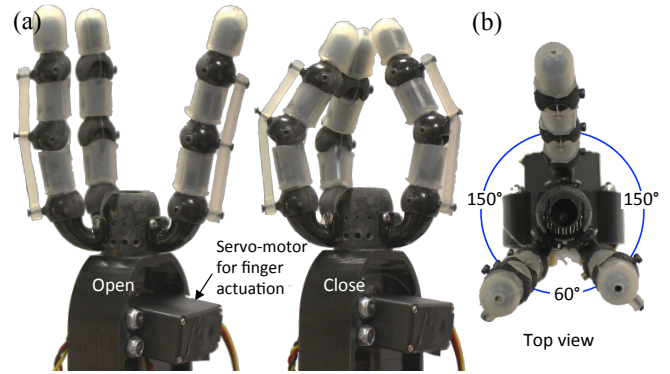state was poured into three different 3-D printed molds for the three finger nodes and cured at room temperature. When assembled with the bones in a finger, the cured skins were put on after the active tendon was routed through. Fig. 5 shows the actual molds used for the skin fabrication and cured skin in the molds.

C. FBG embedment

1) FBGs in Bone: Since optical fibers cannot be directly embedded during the 3-D printing process of fingers, they had to be embedded via a post process. Fig. 6-a shows the finger bone and its joint design. The longitudinal grooves (width: 650 μm, depth: 830 μm) wrap around the tip of each bone, with a bend radius of 5 mm. Due to the small bend radius, bend insensitive optical fibers (Corning ZBL) were selected in our prototype to minimize optical power loss associated with such small bends. These grooves allow multiplexed sensor pairs for each fiber along the sensing axes. Optical fibers were embedded only in the fingertip and finger-base grooves. In addition to the grooves, the middle and base bones contain multiple slots (width: 1 mm) for internal routing of the optical fibers. While the fiber embedding grooves are shallow, the fiber routing slots are through the bone material.

Optical fibers are routed through the slots and inserted in the grooves. The low viscosity of the cyanoacrylate glue we used made the glue quickly flow between the fiber and the groove surface making a strong bond between the two. During this process, the FBGs should be placed at the desired locations on the finger before gluing.

2) FBGs in Skin: The FBGs for the skin are embedded during the casting process, as shown in Fig. 6-b. Since the optical fibers could not be fixed in the middle of the uncured silicone volume, the fibers with FBGs were first glued to a thin and flexible support structure, a Kapton® tape (thickness: 30 μm) tube, that had a diameter of 12 mm, the average of the inner (10 mm) and outer (14 mm) diameters of the skin. This Kapton® tube with optical fibers was inserted in the mold before liquid silicone was poured. The Kapton® tube structure ensured that the fibers were buried in the skin and not exposed at the surface of the skin. It also prevented
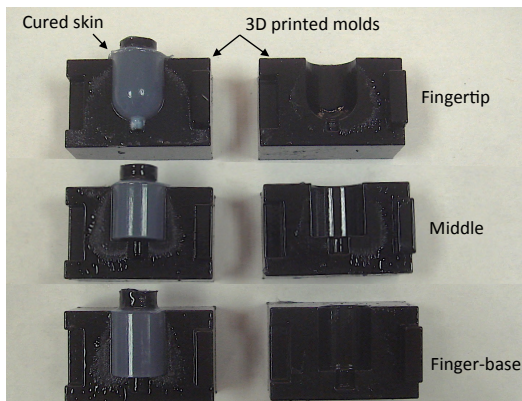
Fig. 5. 3-D printed molds for soft skin fabrication and cured skins in the molds.
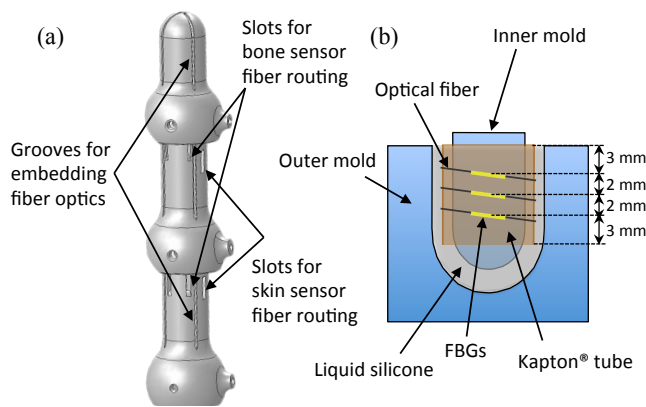

Fig. 6. Fiber optics embedding techniques. (a) Bone structure with multiple grooves and slots. (b) Soft skin casting process with fiber optics attached to a support structure (Kapton® tube).

the fibers from making any direct contact with the finger bone during the curing of silicone.

3) Fiber Optics Connection: Four FBG sensors on each finger node (fingertip or finger-base) were multiplexed along one fiber on each node, and three FBG sensors on each skin node (fingertip or finger-base) were multiplexed along one fiber on each node. This limits the number of required fiber connectors to four (two for bone sensors and the other two for skin sensors) to match the four input ports available at the FBG interrogator (I*Sense^{TM}, Intelligent Fiber Optic Systems) used in this work, which can sample FBG signals at up to 6 kHz for a single fiber .

IV. CHARACTERIZATION

A. Contact Force Sensing

Fig. 7 shows the experimental setups for two different calibration tests: *x* and *y*-axis force tests. The fingers were attached to the hand-base using machine screws and a friction fit. The base itself was clamped such that the load was perpendicular to the fingertip surface. Calibration weights were hung from the end of the fingertip using a thin string. Overall, the setup for this test was simple yet effective.
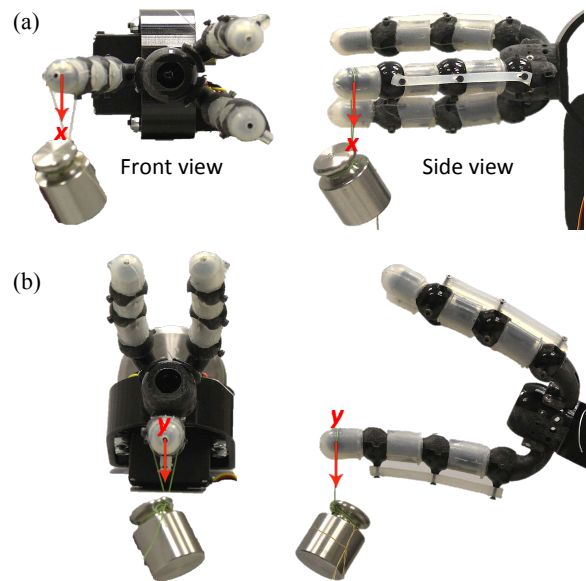

Fig. 7. Experimental setup for contact force calibration. (a) *x*-axis force calibration. (b) *y*-axis force calibration.

The force responses of the finger sensors located on the fingertip and finger-base were measured by applying forces in the *x* and *y* directions. The fingertip was gradually loaded with masses that were hung in increments of 30 g (0.29 N in force) up to 300 g (2.9 N in force) from the edge of the finger tip. The wavelength differences for fibers 1-4 were recorded, and the results showed linearity in force sensing as shown in Figs. 8 and 9. The wavelength differentials $\Delta(\lambda_a - \lambda_b)$ were measured to eliminate the changes in wavelength due to the change in temperature and to use two different FBGs for simple but accurate estimation. Taking differentials also bolsters the sensitivity because each FBG is in either tension or compression, thus creating a large wavelength difference which increases the sensitivity of the sensors. The data of the finger-base showed much higher sensitivity and linearity than those of the fingertip due to the longer moment arm of the applied force and a more stable joint structure, respectively.

B. Contact Localization

The soft skins for the fingertip and finger-base nodes have six embedded FBG sensors (three FBGs in each node) for tactile sensing. When the finger touches an object, the three skin FBGs detect the deformations of the skin and provide information on the location of the contact. To check the tactile sensing capability, a cylindrical rigid object (diameter: 3 mm) was slowly rolled with a light normal force (1~2 N) in the axial direction of the finger, as shown in Fig. 10-a. During this test, the wavelength shifts from the three sensors were measured and the contact location of the object was estimated based on the centroid method [9], [32]. The test was repeated five times, and the results are shown in Fig. 10-b. The current method estimated the middle point close to the real location. However, the beginning and end points were overestimated and underestimated, respectively.
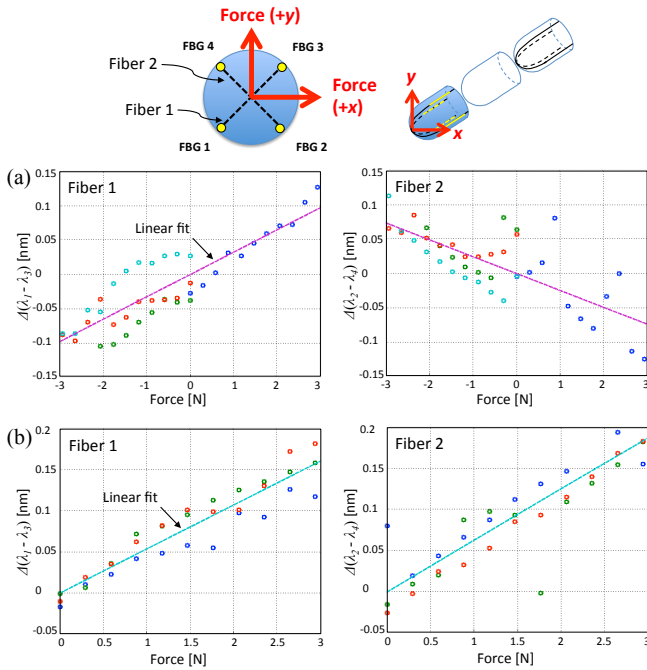
Fig. 8. Fingertip force calibration results using fibers 1 and 2. (a) *x*-axis force calibration. (b) *y*-axis force calibration. Color of the data points represent the different sets of experiments.

Fig. 9. Finger-base force calibration results using fiber 3 and 4. (a) *x*-axis force calibration. (b) *y*-axis force calibration. Color of the data points represent the different sets of experiments.

C. Hysteresis Analysis

Since the fingers were made of polymer materials, they are expected to show creep when an external force was applied to the structure for a period of time, as previously described in [9], [33]. Two 5-minute calibration tests for an loading and unloading loop in *x*-axis were conducted to characterize the hysteresis level of the finger. The wavelength shifts were measured from fibers 3 and 4 embedded at the finger-base. The result, shown in Fig. 11, demonstrated that the finger experienced higher hysteresis when larger forces were applied. However, the levels became lower when the load gradually decreased.

V. CONCLUSION AND FUTURE WORK

The main contribution of this work is design of a multi-fingered robotic hand with a combination of rigid and soft materials with implementation of fiber optic force and tactile sensing. While the sensors in the rigid structure detect accurate forces applied to the hand, the sensors in the soft skin provide information on the location of the contact points.

Although fiber optic strain sensors have been implemented for detecting structural deformations of robotic fingers for force sensing previously [9], [33], [34], this was only for single finger force sensing. By contrast, the work presented in this paper showed the design and experimental results of a multi-fingered hand and demonstrated a potential for expansion of our design concept to more complex multi-joint systems. The fiber optic sensors not only enabled simple and lightweight structures, but also provided accurate measurement of contact forces. Moreover, the soft skin was
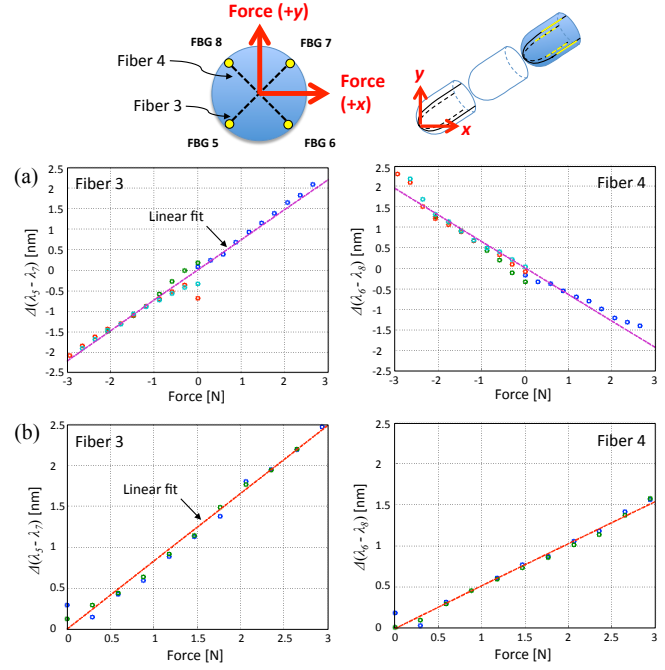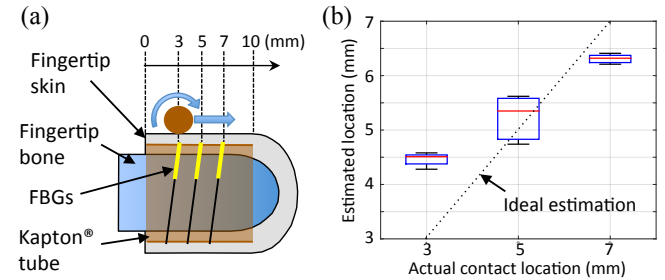

Fig. 10. Contact localization experiment. (a) Experimental setup and procedure. (b) Contact location estimation result.

able to estimate the location of the contacts through the embedded array of fiber optic sensors.

To increase the sensitivity and accuracy of tactile sensing capability, we will increase the density of skin sensors, in both the longitudinal and latitudinal directions. The middle node of the finger will also be sensorized with more sensors.

The current work mainly focused on the design and characterization of the fingers, not including any control results. However, development of control algorithms for both force and position control is currently under investigation. Once the control algorithms are ready, manipulation tests with various objects in terms of shape and weight will be performed. We expect the high sensitivity of FBG sensors will enable various dexterous manipulation tasks.

One immediate area of future work is to eliminate hysteresis of sensing, mainly caused by creep of the polymer finger
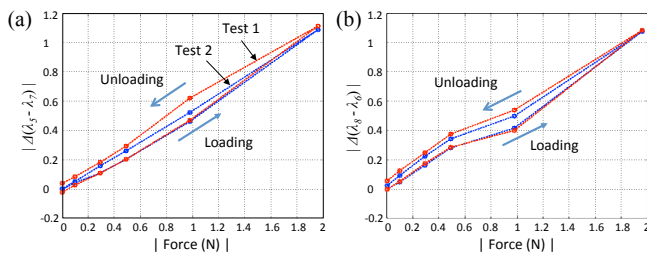
Fig. 11. Hysteresis analysis results for *x*-axis loading and unloading input at the finger-base for (a) fiber 3 and (b) fiber 4.

structures. By embedding or glueing reinforcement materials, such as carbon fiber or metal mesh, we will be able to reduce the hysteresis and increase the sensing accuracy of the hand.

Another area of future work is stiffness control of passive tendons. The two passive tendons of our current finger have the same stiffness, providing only one gripping motion. However, if we use variable stiffness materials for the passive tendons, we will be able to create different gripping motions for different applications.

REFERENCES

[1] D. Trivedi, C. D. Rahn, W. M. Kier, and I. D. Walker, "Soft robotics: biological inspiration, state of the art, and future research," *Biol. Inspired Rob. Mech. 1*, vol. 5, no. 3, 2008.

[2] S. Kim, C. Laschi, and B. Trimmer, "Soft robotics: a bioinspired evolution in robotics," *Trends Biotechnol.*, vol. 31, no. 5, pp. 287–294, 2013.

[3] W. Bluethmann, R. Ambrose, M. Diftler, S. Askew, E. Huber, M. Goza, F. Rehnmark, C. Lovchik, and D. Magruder, "Robonaut: A robot designed to work with humans in space," *Auton. Rob.*, vol. 14, no. 2-3, pp. 179–197, 2003.

[4] R. O. Ambrose, H. Aldridge, R. S. Askew, W. Bluethmann, M. Diftler, C. Lovchik, D. Magruder, and F. Rehnmark, "Robonaut: NASA's space humanoid," *IEEE Intell. Syst.*, vol. 15, no. 4, pp. 57–63, 2000.

[5] T. A. Keil, "Functional morphology of insect mechanoreceptors," *Microsc. Res. Tech.*, vol. 39, no. 6, pp. 506–531, 1997.

[6] F. G. Barth, "Spider mechanoreceptors," *Curr. Opin. Neurobiol.*, vol. 14, no. 4, pp. 415–422, 2004.

[7] D. Alba, M. Armada, and R. Ponticelli, "An introductory revision to humanoid robot hands," *Climbing and Walking Rob.*, pp. 701–712, 2005.

[8] R. Franke, J. Malzahn, T. Nierobisch, F. Hoffmann, and T. Bertram, "Vibration control of a multi-link flexible robot arm with fiber-Bragg-grating sensors," in *Proc. IEEE Int. Conf. Rob. Autom. (ICRA'09)*, 2009, pp. 3365–3370.

[9] Y.-L. Park, S. C. Ryu, R. J. Black, K. Chau, B. Moslehi, and M. R. Cutkosky, "Exoskeletal force-sensing end-effectors with embedded optical fiber-bragg-grating sensors," *IEEE Trans. Rob.*, vol. 25, no. 6, pp. 1319–1331, December 2009.

[10] Y.-L. Park, S. Elayaperumal, B. Daniel, S. C. Ryu, M. Shin, J. Savall, R. J. Black, B. Moslehi, and M. R. Cutkosky, "Real-time estimation of 3-D needle shape and deflection for mri-guided interventions," *IEEE/ASME Trans. Mechatron.*, vol. 15, no. 6, pp. 906–915, 2010.

[11] H. Su, M. Zervas, G. A. Cole, C. Furlong, and G. S. Fischer, "Real-time MRI-guided needle placement robot with integrated fiber optic force sensing," in *Proc. IEEE Int. Conf. Rob. Autom. (ICRA'11)*, Shanghai, China, May 2011, pp. 1583–1588.

[12] H. R. Nicholls and M. H. Lee, "A survey of robot tactile sensing technology," *Int. J. Rob. Res.*, vol. 8, no. 3, pp. 3–30, 1989.

[13] M. H. Lee and H. R. Nicholls, "Review article tactile sensing for mechatronics—a state of the art survey," *Mechatron.*, vol. 9, no. 1, pp. 1–31, 1999.

[14] P. Puangmali, K. Althoefer, L. D. Seneviratne, D. Murphy, and P. Dasgupta, "State-of-the-art in force and tactile sensing for minimally invasive surgery," *IEEE Sens. J.*, vol. 8, no. 4, pp. 371–381, 2008.

[15] W. Fukui, F. Kobayashi, F. Kojima, H. Nakamoto, N. Imamura, T. Maeda, and H. Shirasawa, "High-speed tactile sensing for array-type tactile sensor and object manipulation based on tactile information," *J. Rob.*, p. 691769, 2011.

[16] H. Kawasaki, T. Komatsu, and K. Uchiyama, "Dexterous anthropo-morphic robot hand with distributed tactile sensor: Gifu hand II," *IEEE/ASME Trans. Mechatron.*, vol. 7, no. 3, pp. 296–303, 2002.

[17] M. Shimojo, T. Suzuki, A. Namiki, T. Saito, M. Kunimoto, R. Makino, H. Ogawa, M. Ishikawa, and K. Mabuchi, "Development of a system for experiencing tactile sensation from a robot hand by electrically stimulating sensory nerve fiber," in *Proc. IEEE Int. Conf. Rob. Autom. (ICRA'03)*, vol. 1, Taipei, Taiwan, September 2003, pp. 1264–1270.

[18] A. D. Kersey, M. A. Davis, H. J. Patrick, M. LeBlanc, K. P. Koo, C. G. Askins, M. A. Putnam, and E. J. Friebele, "Fiber grating sensors," *J. Lightwave Technol.*, vol. 15, no. 8, pp. 1442–1463, 1997.

[19] K. O. Hill and G. Meltz, "Fiber Bragg grating technology fundamen-tals and overview," *J. Lightwave Technol.*, vol. 15, no. 8, pp. 1263–1276, 1997.

[20] R. Kashyap, *Fiber Bragg gratings*. Academic Press, 1999.

[21] T. Laliberte, L. Birglen, and C. M. Gosselin, "Underactuation in robotic grasping hands," *Mach. Intell. Rob. Control*, vol. 4, no. 3, pp. 1–11, 2002.

[22] B. Massa, S. Roccella, M. C. Carrozza, and P. Dario, "Design and development of an underactuated prosthetic hand," in *Proc. IEEE Int. Conf. Rob. Autom. (ICRA'02)*, 2002, pp. 3374–3379.

[23] S. Kim, M. S. Spenko, S. Trujillo, B. Heyneman, D. Santos, and M. R. Cutkosky, "Smooth vertical surface climbing with directional adhesion," *IEEE Trans. Rob.*, vol. 24, no. 1, pp. 65–74, 2008.

[24] M. R. Cutkosky and S. Kim, "Design and fabrication of multi-material structures for bioinspired robots," *Phil. Trans. R. Soc. A*, vol. 367, no. 1894, pp. 1799–1813, 2009.

[25] A. M. Dollar and R. D. Howe, "Joint coupling design of underactuated hands for unstructured environments," *Int. J. Rob. Res.*, vol. 30, no. 9, pp. 1157–1169, 2011.

[26] G.-P. Jung, J.-S. Koh, and K.-J. Cho, "Underactuated adaptive gripper using flexural buckling," *IEEE Trans. Rob.*, vol. 29, no. 6, pp. 1396–1407, 2013.

[27] R. P. Lane, *Medical Insects and Arachnids*. Springer Science+Business Media, 1993, ch. Introduction to the arthropods, pp. 30–47.

[28] J. D. Currey, "The failure of exoskeletons and endoskeletons," *J. Morphol.*, vol. 123, no. 1, pp. 1–16, 2005.

[29] R. R. Maier, W. N. MacPherson, J. S. Barton, J. D. C. Jones, S. McCulloch, and G. Burnell, "Temperature dependence of the stress response of fibre bragg gratings," *Meas. Sci. Technol.*, vol. 15, no. 8, 2004.

[30] R. J. Black, D. Zare, L. Oblea, Y.-L. Park, and B. Moslehi, "On the gage factor for optical fiber grating strain gages," in *Proc. Int. Symp. Exhibition, Soc. Adv. Mater. Process Eng. (SAMPE'08)*, vol. 53, Long Beach, CA, May 2008.

[31] R. J. Black, J. M. Costa, B. Moslehi, and V. Sotoudeh, "Broad-band fiber Bragg grating interrogation for structural health monitor-ing," in *Proc. Int. Symp. Exhibition, Soc. Adv. Mater. Process Eng. (SAMPE'15)*, Baltimore, MD, May 2015.

[32] J. S. Son, M. R. Cutkosky, and R. D. Howe, "Comparison of contact sensor localization abilities during manipulation," in *Proc. IEEE/RSJ Int. Conf. Intell. Rob. Syst. (IROS'95)*, vol. 2, Pittsburgh, PA, August 1995, pp. 96–103.

[33] Y.-L. Park, S. C. Ryu, R. J. Black, B. Moslehi, and M. R. Cutkosky, "Fingertip force control with embedded fiber bragg grating sensors," in *Proc. IEEE Int. Conf. Rob. Autom. (ICRA'08)*, Pasadena, CA, May 2008, pp. 3431–3436.

[34] Y.-L. Park, K. Chau, R. J. Black, and M. R. Cutkosky, "Force sensing robot fingers using embedded fiber bragg grating sensors and shape deposition manufacturing," in *Proc. IEEE Int. Conf. Rob. Autom. (ICRA'07)*, Roma, Italy, April 2007, pp. 1510–1516.